

recoil protons have the highest energy and are most easily resolved from the background events.

The measured cross sections can be seen to agree reasonably well with those calculated except for the persistently low point at 310 MeV for 90° . The experimental errors, however, are too large to provide a reliable check on the CGLN value of ρ . It seems that the remaining uncertainties in the interpretation of the proton Compton effect in this energy region could be resolved most clearly by a detailed measurement of the angular distribution at the resonance energy.

ACKNOWLEDGMENTS

We wish to acknowledge the contributions of Dr. Lutz Criegee in planning this work, of Dr. John Dana Fox in assembling and testing the experimental equipment, and of Steve Kiergan and John Staples, who assisted in all stages of the work. We are indebted to Dr. Roy Schult for discussions regarding the theoretical calculations and to Dr. A. P. Contogouris for supplying us with the unpublished calculations for the cross sections at 135° .

Photoproduction of Charged Pion Pairs and $N^*(1238)^{++}$ in Hydrogen from 0.9 to 1.3 GeV*

M. G. HAUSER†

California Institute of Technology, Pasadena, California

(Received 31 March 1967)

The momentum spectrum of negative pions produced in the reaction $\gamma + p \rightarrow \pi^- + \pi^+ + p$ has been measured at eight photon laboratory energies from 0.9 to 1.3 GeV at c.m. angles from 7° to 150° . The reaction was produced in a liquid-hydrogen target illuminated by a bremsstrahlung beam from the Caltech synchrotron. The π^- were detected and momentum analyzed with a magnetic spectrometer employing a combination of scintillation counters and Cherenkov counters. The incident photon energy was fixed by using the technique of bremsstrahlung subtraction. The cross section for the pseudo-two-body reaction $\gamma + p \rightarrow \pi^- + N^*(1238)^{++}$ was obtained by fitting the π^- momentum spectrum at each angle and energy with a linear combination of a resonance term and three-body phase space. The angular distribution of the π^- in N^* production shows the small-angle peak and decrease near 0° predicted by the one-pion-exchange (OPE) model. Gauge-invariant models are in poorer agreement with the data. Moravcsik fits to the angular distributions are presented, and are extrapolated to obtain a value for the πNN^* coupling constant of $23.1 \pm 2.0 \text{ GeV}^{-2}$, in fair agreement with the value obtained from the width of the $N^*(1238)$. The total cross section for pion pair production decreases smoothly from $78.9 \pm 2.9 \mu\text{b}$ at 0.93 GeV to $59.1 \pm 5.2 \mu\text{b}$ at 1.29 GeV, whereas the N^* part of the cross section decreases from $45.0 \pm 2.4 \mu\text{b}$ to $18.2 \pm 3.5 \mu\text{b}$ over the same range. There is no strong evidence for formation of the $N^*(1688)$ as an intermediate state.

I. INTRODUCTION

EVIDENCE for the photoproduction of charged pion pairs from hydrogen, $\gamma + p \rightarrow \pi^- + \pi^+ + p$, was first reported in 1954.¹ Although numerous experimental investigations of this process have been made since then, only in the past few years have sufficient data been obtained to permit comparison with the detailed predictions of dynamical models. This paper gives the results of a counter experiment in which momentum spectra and angular distributions of negative pions produced in this reaction were measured for incident photon energies from 0.9 to 1.3 GeV.

A model for the mechanism of this reaction was proposed by Drell in an investigation of the production of beams of high-energy particles.² The Drell model, or one-pion-exchange (OPE) model, is based upon the

amplitude given by the Feynman diagram shown in Fig. 1. This model predicts that the angular distribution of the π^- will be peaked strongly forward, but that the cross section should be small at 0° since the contribution of the OPE diagram vanishes there. In the pole approximation, the lower vertex in Fig. 1 is given by the $\pi^+ - p$ scattering amplitude for real pions, which is dominated by the $N^*(1238)$ at low excitation energies.

The interesting features predicted by this model prompted Kilner, Diebold, and Walker³ to study π^-

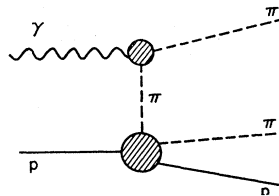


FIG. 1. Diagram for the one-pion-exchange model of pion-pair photoproduction.

* Work supported in part by the U. S. Atomic Energy Commission. Prepared under Contract No. AT(11-1)-68 for the San Francisco Operations Office, U. S. Atomic Energy Commission.

† Now at Princeton University, Princeton, New Jersey.

¹ V. Peterson and I. G. Henry, Phys. Rev. **96**, 850 (1954).

² S. D. Drell, Phys. Rev. Letters **5**, 278 (1960).

³ J. R. Kilner, R. E. Diebold, and R. L. Walker, Phys. Rev. Letters **5**, 518 (1960).

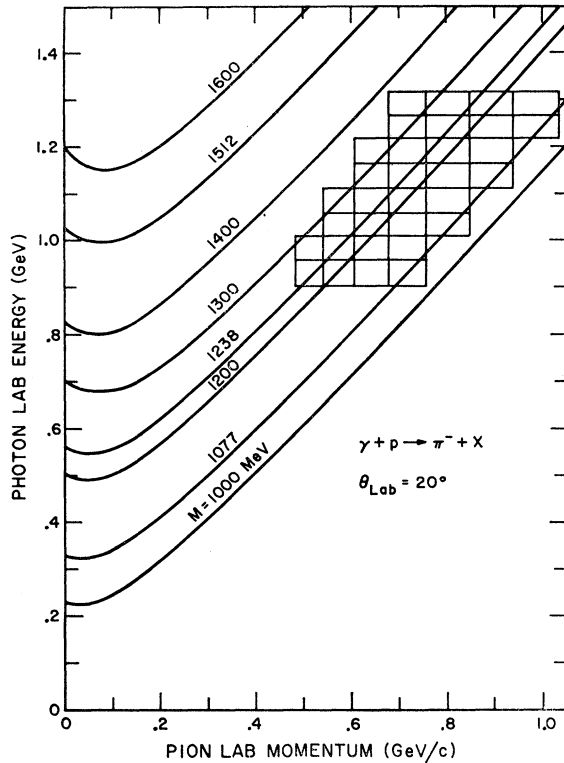


FIG. 2. Laboratory kinematics for photoproduction of a negative pion from hydrogen at a laboratory angle of 20° . The smooth curves are lines of constant invariant mass of all final-state particles other than the detected pion. Each block shows the range covered in a single bremsstrahlung subtraction and setting of the spectrometer central momentum. The momentum acceptance shown was divided into four channels by a counter hodoscope on the spectrometer.

production from hydrogen at small angles at an incident photon energy of 1.23 GeV. They found that the cross section exhibits the qualitative features of the Drell model, but is a factor of 2 or 3 larger than the prediction. The striking qualitative agreement between their data and Drell's predictions suggests that it would be very interesting to extend the measurements over a greater energy and angular range. In addition, one might expect the Drell model to be more successful in describing the reaction $\gamma + p \rightarrow \pi^- + N^*(1238)^{++}$ than in describing all charged pion-pair photoproduction. Investigations in which this quasi-two-body channel was isolated were recently completed by the bubble-chamber collaborations at CEA⁴ and DESY^{5,6} for energies from threshold to 5.5 GeV, and by a counter group at Stanford⁷ for energies from 0.57 to

⁴ H. R. Crouch *et al.*, in *Proceedings of the International Symposium on Electron and Photon Interactions at High Energies* (Deutsche Physikalische Gesellschaft, Hanau, Germany, 1966), Vol. II.

⁵ U. Brall *et al.*, *Nuovo Cimento* 41, 270 (1966).

⁶ German Bubble-Chamber Collaboration, in *Proceedings of the Thirteenth International Conference on High-Energy Physics, Berkeley, 1966* (University of California Press, Berkeley, California, 1967).

⁷ J. V. Allaby, H. L. Lynch, and D. M. Ritson, *Phys. Rev.* 142, 887 (1966).

0.95 GeV. The work reported here extends the counter measurements through the energy range where $N^*(1238)$ production is the dominant part of pion-pair production. In this energy range we could also look for evidence of the effect of the third pion-nucleon resonance, $N^*(1688)$, on pion-pair production.

This paper is divided into five parts. Section II summarizes the experimental method. The apparatus is described in Sec. III. The analysis of the data is considered in Sec. IV, where the data are also presented. The results of this experiment are discussed and compared with other recent experiments and predictions of the OPE model in Sec. V.

II. EXPERIMENTAL METHOD

A. Procedure

The method of investigation employed in this experiment has been used in several previous studies of pion-pair photoproduction.^{3,7,8} Negative pions photoproduced in a liquid-hydrogen target by a bremsstrahlung beam from the Caltech synchrotron were detected and their momentum (p) and direction (θ) were measured with a magnetic spectrometer. Because this information does not suffice to determine the photon energy (k), data were taken in such a way that a bremsstrahlung subtraction could be performed: The π^- yields obtained at a fixed angle and momentum but slightly different synchrotron energies were subtracted. The net yield of pions was produced by photons whose energy was known to lie in a relatively narrow band. The increment in synchrotron energy used in this experiment was 50 MeV, chosen as a compromise between the desire to minimize random errors and the desire to obtain the best possible resolution in total c.m. energy (W).

The laboratory cross section measured as outlined above is differential in both pion momentum and angle. At fixed k and θ , this cross section is essentially a spectrum of the invariant mass of all undetected final-state particles, hereafter referred to as the missing mass (M). This can be visualized by considering the kinematics for the reaction in the manner shown in Fig. 2, where contours of M are shown in the k - p plane for fixed θ .

For each angle at which the cross section was measured, a set of standard momentum values, separated by slightly more than the spectrometer acceptance, was selected. The π^- yield was measured at two synchrotron energies differing by 50 MeV, and at a subset of these standard momentum values such that after the bremsstrahlung subtraction the missing mass varied from its value at the threshold for pion-pair production (1.08 GeV/ c^2) to about 1.30 GeV/ c^2 . These measurements were made at nine synchrotron energies from 922 to 1330 MeV, and a bremsstrahlung subtraction was per-

⁸ M. Bloch and M. Sands, *Phys. Rev.* 113, 305 (1959).

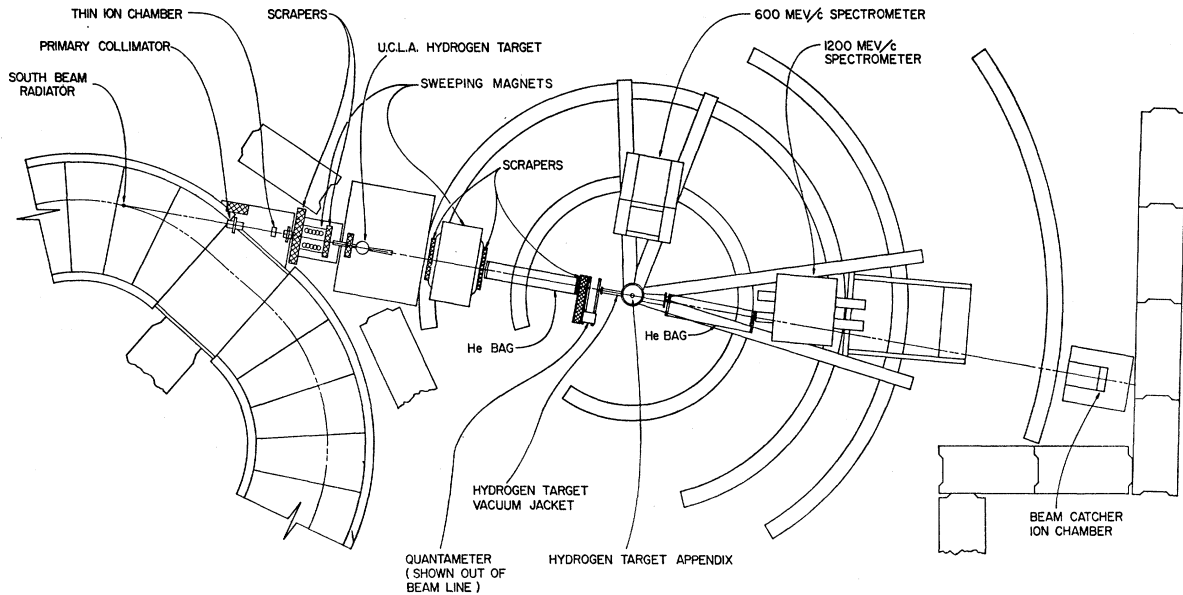


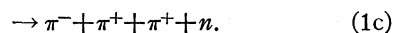
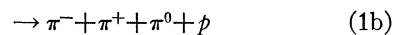
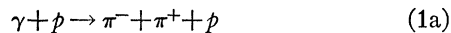
Fig. 3. Arrangement of experimental apparatus during the second half of the experiment. During the first half of the experiment, the sweeping magnet and helium bags close to the hydrogen target were not present.

formed at each pair of adjacent energies, the result being cross-section measurements at eight average photon energies from 934 to 1289 MeV. The regions blocked out in Fig. 2 show the kinematic points selected in a typical case. The cross section was measured in this manner at laboratory angles of 4° , 12° , 20° , 44° , 56° , and 84° . Additional measurements were made at 30° and 120° over a limited part of the photon-energy range.

Momentum spectra calculated from a phenomenological model were fitted to the laboratory cross sections thus obtained to determine c.m. cross sections and to separate the cross section for the pseudo-two-body channel $\gamma + p \rightarrow \pi^- + N^*(1238)^{++}$ from the complete pion-pair cross section. Angular distributions for the π^- in the c.m. system and total cross sections for charged-pion-pair and $(\pi^- - N^*)$ production were also determined. A detailed discussion of the data analysis is given in Sec. IV.

B. Reaction Identification

Reactions in which negative pions are photoproduced from hydrogen are of the form $\gamma + p \rightarrow \pi^- + X$, where charge conservation requires that X represent at least two particles. Since we limited the maximum photon energy to 1.33 GeV and the maximum invariant mass of the X to $1.3 \text{ GeV}/c^2$, the only reactions which could contribute to our measured cross sections are as follows:



The combined contribution of reactions (1b) and (1c) to the negative-pion total cross section we observed is estimated to be about $1 \mu\text{b}$ at all energies, less than 2% of the total cross section. This estimate is based upon published total cross sections for the three-pion reactions⁵ and the assumption that invariant phase space adequately describes the missing-mass distribution for these reactions. The good agreement between our total cross sections and those for pion-pair production obtained in the bubble chamber studies gives us confidence that we have not seriously underestimated the three-pion contribution. We therefore believe that we have measured the cross section for reaction (1a) alone.

III. APPARATUS

A. Photon Beam

The arrangement of experimental equipment is shown in Fig. 3. The bremsstrahlung beam produced in a 0.2-radiation-length tantalum radiator was collimated to a rectangular cross section with half-angles of 1.8 mrad horizontally and 2.2 mrad vertically. The central beam was not further collimated, but several lead scraping walls removed photons and charged particles diverging from the beam line. During the first half of the experiment, a single sweeping magnet, located just downstream from the primary collimator, was used to deflect charged particles from the beam. In the second half of the experiment, an additional sweeping magnet with scraping walls at its entrance and exit was added closer to our hydrogen target. A helium bag from the exit of this magnet to the entrance window of the hydrogen-target vacuum jacket also helped to reduce the charged-particle content of the beam.

There were two properties of the beam which had to be known accurately in order to minimize random errors in this experiment: the total energy in the beam during each run, and the change in synchrotron energy from one run to the next. The bremsstrahlung subtraction tended to amplify small errors in these quantities. In addition, inaccuracies in the shape of the bremsstrahlung spectrum and in the absolute calibration of the synchrotron energy were potential sources of systematic error. The methods used to determine each of these properties of the beam are described below.

The total energy of the bremsstrahlung beam in each run was monitored with several secondary monitors, including a thin (0.005-in.-Al) ionization chamber and a probe measuring the circulating beam in the synchrotron. These monitors were calibrated absolutely using a Wilson quantameter⁹ before and after every run. Analysis of many runs taken under identical conditions showed that this method of beam monitoring introduced an rms fluctuation of 1% into the counting rates. This was generally a small random error compared with that resulting from counting statistics. The calibration constant of the quantameter was found to be in good agreement with the calculated value in a comparison with a Faraday cup performed at Stanford when this experiment was partly completed.¹⁰

The energy of the internal electron beam is determined by measuring the field of the synchrotron magnet. The energy meter was calibrated electronically¹¹ and by measuring excitation curves for the reaction $\gamma + p \rightarrow \pi^+ + n$ with the magnetic spectrometers used in this experiment.^{10,12} These calibrations were in good agreement, and determined the synchrotron energy with an estimated accuracy of $\frac{1}{2}$ %.

The accuracy of the effective increment in synchrotron energy from one run to the next depended upon the differential linearity of the beam-energy meter, since it was used to adjust the peak field of the synchrotron magnet, and upon the reproducibility of the peak field from one machine cycle to the next. (The magnetic field was constant during a single beam dump to better than 0.2%.) The beam-energy meter was found to have a maximum error of 2 MeV for a 50-MeV change, and the synchrotron energy rarely drifted by more than 2 MeV once the operating conditions were set. In order to be as insensitive as possible to long-term drifts, data were obtained as energy scans at fixed p and θ .

The shape of the bremsstrahlung spectrum was computed using a theory of thick-radiator bremsstrahlung developed by Wolverson.¹³ The photon distribu-

tion, differential in energy and angle, was integrated over the aperture defined by our primary collimator to obtain the spectrum. Wolverson estimates his calculation is accurate within 2%. We believe that the error in the area of the net bremsstrahlung spectrum was dominated by uncertainties in the synchrotron energy, and not by inaccuracies in the spectrum.

B. The Hydrogen Target and Spectrometers

The hydrogen target used in this investigation has been employed in many previous experiments.^{10,12} The liquid hydrogen is contained in a cylindrical (3-in.-diameter) Mylar cup, with its axis normal to the direction of the bremsstrahlung beam.

Two magnetic spectrometers viewed the hydrogen target; they were operated independently to measure the π^- yield at two angles simultaneously. Each of these spectrometers consisted of a wedge shaped, uniform-field magnet and a system of scintillation counters and Cherenkov counters. The 1200 MeV/ c spectrometer was used to measure the π^- yield from 4° to 44° in the laboratory, over a momentum range of 450 to 1200 MeV/ c . The counter system of this spectrometer included a freon threshold Cherenkov counter which effectively provided 100% discrimination against the large electron flux at small angles. The 600 MeV/ c spectrometer was used to measure the yield from 30° to 120° , covering a momentum range of 250 to 600 MeV/ c . A counter to discriminate against electrons was not included on this spectrometer, resulting in a contamination of the cross section estimated to be less than 5% in the worst case (largest angle). The 600 MeV/ c spectrometer, including the counters and associated electronics, has recently been described by Thiessen¹⁰; a description of the 1200-MeV/ c spectrometer was given by Ecklund and Walker.¹² These authors also described the techniques used to determine the momentum calibration and resolution functions of the spectrometers. It should be emphasized that the resolution functions of the spectrometers were accurately known, enabling us to make an absolute cross-section measurement.

IV. RESULTS

A. Yield

We define the negative-pion yield per equivalent quantum, σ^* , as follows:

$$\sigma^*(E_0, p, \theta) = E_0 \int_{k_m}^{E_0} dk N(k, E_0) \frac{d^2\sigma}{dpd\Omega}, \quad (2)$$

where E_0 = synchrotron energy, $k_m(p, \theta)$ = minimum photon energy required to produce a π^- of momentum p at angle θ , $N(k, E_0)dk$ = number of photons with energy in the interval k to $k+dk$ per unit energy of the beam, $d^2\sigma/dpd\Omega(k, p, \theta)$ = laboratory cross section for

⁹ R. R. Wilson, Nucl. Instr. Methods **1**, 101 (1957).

¹⁰ H. A. Thiessen, Phys. Rev. **155**, 1488 (1967).

¹¹ H. A. Thiessen, California Institute of Technology Synchrotron Laboratory Internal Report No. CTSL-21, 1966 (unpublished).

¹² S. D. Ecklund and R. L. Walker, Phys. Rev. **159**, 1195 (1967).

¹³ An account of this work is in preparation. F. B. Wolverson kindly provided a computer program for performing the calculations.

π^- production per unit momentum and unit solid angle by a photon of energy k . This quantity, which has the dimensions of a cross section per unit momentum and solid angle, was computed from the counting rates and known instrumental parameters:

$$\sigma^*(E_0, \hat{p}, \theta) = \frac{E_0 C}{\eta D \rho_H \Delta \Omega \Delta \hat{p}}, \quad (3)$$

where $C(E_0, \hat{p}, \theta)$ = number of π^- counted per unit energy of the photon beam, η = pion detection efficiency, D = effective length of the hydrogen target, ρ_H = proton density in the target, $\Delta \Omega$ = total angular aperture of the spectrometer, $\Delta \hat{p}$ = total momentum acceptance of the spectrometer. Since the counting rate is actually an integral of σ^* over the momentum and angular resolution functions of the spectrometer, $d^2\sigma/d\hat{p}d\Omega$ must be regarded as the cross section averaged over these functions.

A number of corrections were included in the factors appearing in Eq. (3): (1) The spectrometer acceptance was corrected for pion decay. Since pions and muons were indistinguishable, a Monte Carlo program was used to calculate the acceptance for pions which decay in flight. The cutoff for the high-momentum tail of this resolution function was determined from the kinematics of pion-pair production. The net correction to the stable-particle resolution function was typically 10%. (2) Nuclear scattering of pions in the matter along their flight path caused a loss of events. The π^+ attenuation was determined for the spectrometers by Thiessen¹⁰ and by Ecklund and Walker.¹² The π^- attenuation was obtained from their results by taking account of differences in the π^+ and π^- scattering cross sections. The correction varied from 5% to 10% for the 600-MeV/c spectrometer, and from 10% to 13% for the 1200-MeV/c spectrometer. (3) Accidental coincidences, deadtime losses, and other electronic inefficiencies were less than 2%. (4) A correction for the cylindrical geometry of the hydrogen target was included in the calculation of the integral of the bremsstrahlung spectrum over the collimator aperture. With this procedure, D was just the diameter of the hydrogen target.

The yields thus obtained were corrected for pions produced in material other than the liquid hydrogen by subtracting yields measured with the target empty. The empty-target yield varied from 100% of the full-target yield at threshold to as low as about 10% at most angles. At 4°, the empty-target yield was never less than about 30% of the full-target yield because the spectrometer could detect pions produced in the Mylar windows of the hydrogen-target vacuum jacket. The total time spent measuring the background at 4° was nearly equal to the time spent with the target full.

A typical pair of yield curves obtained at a fixed angle is plotted in Fig. 4. These data are for a point

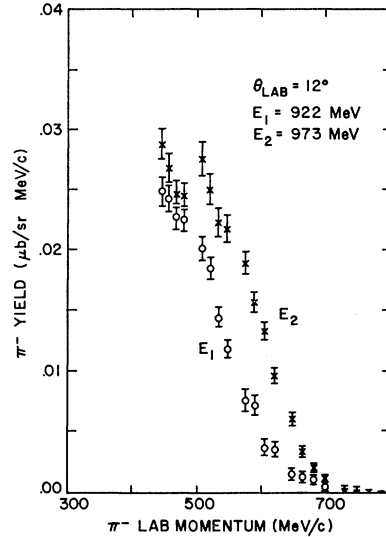


Fig. 4. Typical π^- yield curves obtained at a π^- laboratory angle of 12° with the 1200-MeV/c spectrometer.

where the cross section is large and the bremsstrahlung subtraction was easily made. Note that as the π^- momentum decreases, the bremsstrahlung subtraction becomes more difficult: This behavior sets a practical limit to the largest missing mass which can be observed. Several determinations of σ^* were made at almost all kinematic points, and these different "batches" of data were treated separately until after the bremsstrahlung subtraction was made in order to minimize the effects of systematic changes.

B. Laboratory Cross Section

Subtraction of the expressions for the yields at two synchrotron energies $E_2 > E_1$ gives the following integral equation for the cross section:

$$\begin{aligned} \sigma^*(E_2, \hat{p}, \theta) - \sigma^*(E_1, \hat{p}, \theta) \\ = \int_{k_m}^{E_2} dk R(k, E_1, E_2) (d^2\sigma/d\hat{p}d\Omega), \quad (4) \end{aligned}$$

where

$$\begin{aligned} R(k, E_1, E_2) &= E_2 N(k, E_2) - E_1 N(k, E_1), \\ N(k, E_0) &= (1/E_0) [B(k, E_0)/k]. \end{aligned}$$

The beam spectral function $B(k, E_0)$ for our radiator and collimator, including correction for the cylindrical geometry of the hydrogen target, is shown in Fig. 5(a). The kernel of Eq. (4) which results when $E_2 - E_1 = 50$ MeV is shown in Fig. 5(b). It should be noted that k_m was typically no more than a few hundred MeV below E_2 under the conditions of this experiment, so that the low-energy tail of $R(k, E_1, E_2)$ did not make an appreciable contribution to the integral. The rms width of $R(k, E_1, E_2)$ is about 30 MeV.

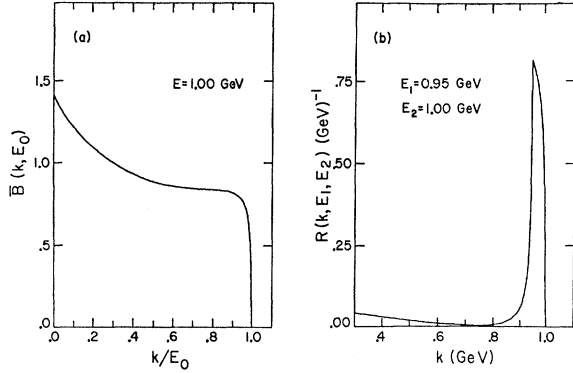


FIG. 5. Bremsstrahlung-beam spectrum functions. (a) $B(k, E_0)$, including correction for the cylindrical geometry of the hydrogen target, for $E_0 = 1$ GeV. (b) Beam spectrum after 50-MeV bremsstrahlung subtraction, normalized to equal numbers of equivalent quanta at each synchrotron energy.

Assuming that the cross section varies slowly with k over the region where $R(k, E_1, E_2)$ is large, we obtain the approximate solution of Eq. (4):

$$\left(\frac{d^2\sigma}{d\phi d\Omega}\right)(k_0, \phi, \theta) \cong \bar{\sigma}(E_2, E_1, \phi, \theta), \quad (5)$$

where

$$\bar{\sigma}(E_2, E_1, \phi, \theta) = [\sigma^*(E_2, \phi, \theta) - \sigma^*(E_1, \phi, \theta)] / I(E_2, E_1, \phi, \theta),$$

$$I(E_1, E_2, \phi, \theta) = \int_{k_m}^{E_2} dk R(k, E_1, E_2),$$

$$k_0 = \left[\int_{k_m}^{E_2} dk k R(k, E_1, E_2) \right] / I(E_2, E_1, \phi, \theta).$$

Equation (5) is obtained by expanding the cross section in a power series about k_0 , and is an exact solution if the cross section varies linearly with k . For reasons discussed below, no attempt was made to evaluate the error incurred as a result of using Eq. (5) to calculate the laboratory cross section.

Some typical cross sections obtained in this way are plotted in Fig. 6. At low energies, the influence of N^{*++} production is quite apparent. The smooth curves in these plots are discussed in the next section. Such momentum spectra were obtained at 57 kinematic points (defined by k_0 and θ). In general, the momentum spectra at angles from 4° through 44° and all energies covered in this experiment show clearly the presence of the N^* . At the larger angles, the cross section becomes so small that the bremsstrahlung subtraction leaves us with large statistical errors. Although the data at 932 and 981 MeV at 56° and 84° still show the N^* fairly well, the separation of the resonant and nonresonant parts of the cross section at higher energies at these angles must be regarded as quite uncertain. The data at 120° are of poorer quality than the rest: A limited set of measurements was made at this angle to determine whether the cross section shows any sign of increasing at the most backward angle we could readily

observe. Since it does not, our data at this angle are statistically poor.

C. Center-of-Mass Cross Section

For purposes of interpretation, it is generally desirable to express the cross section in the center-of-mass (c.m.) system. The laboratory cross section could be multiplied by an appropriate kinematic factor to give the c.m. cross section at corresponding values of the c.m. kinematic variables. We chose a different approach, incorporated in a more physically oriented solution to the unfolding problem presented by Eq. (4) than that provided by Eq. (5).

Rewriting Eq. (4) in terms of the c.m. cross section, we have

$$\bar{\sigma}(E_2, E_1, \phi, \theta) = \left[\int_{k_m}^{E_2} dk R(k, E_1, E_2) J \frac{d^2\sigma'}{dM^2 d\Omega'} \right] / I(E_2, E_1, \phi, \theta), \quad (6)$$

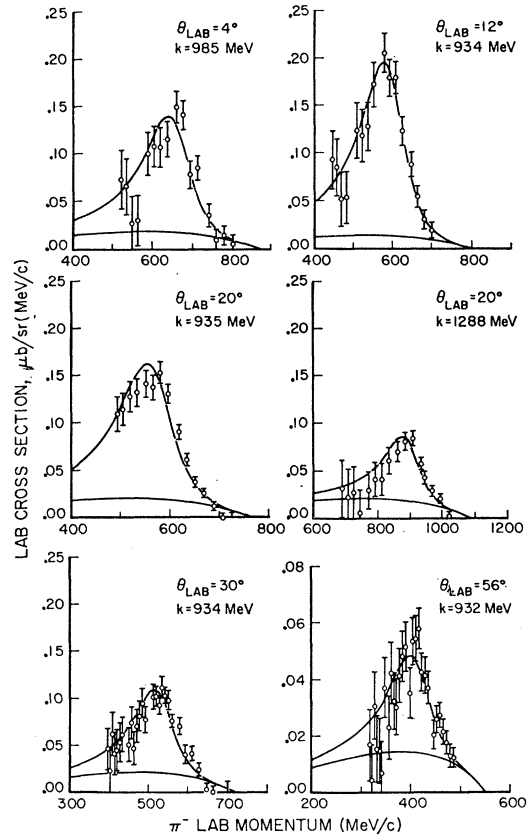


FIG. 6. Sample laboratory cross sections for π^- production, $d^2\sigma/d\phi d\Omega$, obtained by 50-MeV bremsstrahlung subtractions. The data at 4° , 12° , and 20° were measured with the 1200-MeV/c spectrometer; the data at 30° include measurements made with both spectrometers; the 56° data were measured with the 600-MeV/c spectrometer. Note the vertical-scale change at 56° . The upper smooth curve is a least-squares fit of an $N^*(1238)^{++}$ production term plus a three-body phase-space term; the lower curve is the three-body phase-space term alone.

where M = invariant mass of the undetected final-state particles, $(d^2\sigma'/dM^2d\Omega')(k, M^2, \theta') = \text{c.m. cross section for } \pi^- \text{ production per unit solid angle and unit interval of } M^2, \theta' = \pi^- \text{ c.m. angle, } J(k, p, \theta) = \text{Jacobian which transforms this cross section into } d^2\sigma/dp d\Omega \text{ in the lab system. We anticipate that the cross section will have a resonant shape as a function of } M^2. \text{ If } k \text{ and } \theta \text{ are held fixed, this produces a resonant shape as a function of } p, \text{ as shown by the data in Fig. 6. Similarly, if } p \text{ and } \theta \text{ are held fixed, as is the case in Eq. (6), the resonant behavior of the cross section with } M^2 \text{ will produce a resonant shape as a function of } k \text{ (see Fig. 2). In order to solve Eq. (6) without neglecting the finite width of our experimental resolution in } k, \text{ we assume that the most rapid variation of the cross section with } k \text{ is a result of the dependence of the cross section on } M^2, \text{ and expand in functions of } M^2 \text{ and } k \text{ which have the expected resonant behavior or the shape of a phase space background. That is, we take}$

$$\frac{d^2\sigma'}{dM^2d\Omega'} = \sum_{i=1}^n A_i(k, \theta') g_i(M^2, k), \quad (7)$$

where the g_i are functions which will be specified below. We emphasize that we are considering the cross section to be explicitly a function of k , M^2 , and θ' , with an implicit dependence on k , p , and θ through the dependence of M^2 and θ' on these variables.

With this approach, the unknown coefficients $A_i(k, \theta')$ vary quite slowly with k over the region where $R(k, E_1, E_2)$ is large, and Eq. (6) reduces to an algebraic equation:

$$\bar{\sigma}(E_2, E_1, p, \theta) = \sum_{i=1}^n A_i(\bar{k}, \bar{\theta}') F_i(E_2, E_1, p, \theta). \quad (8)$$

The functions F_i , defined by

$$F_i(E_2, E_1, p, \theta) = \left[\int_{k_m}^{E_2} dk R(k, E_1, E_2) J g_i(M^2, k) \right] / I(E_2, E_1, p, \theta), \quad (9)$$

were evaluated numerically. The $A_i(\bar{k}, \bar{\theta}')$ at a single point in (k, θ') space were then obtained by fitting the right side of Eq. (8) at given (E_2, E_1, θ) to the experimental data $\bar{\sigma}(E_2, E_1, p, \theta)$ as a function of p by the method of least squares. The values \bar{k} and $\bar{\theta}'$ were taken, respectively, as averages of k_0 and θ' over the momenta at which $\bar{\sigma}$ was measured. Since we know *a priori* that the cross section should be positive, the A_i were constrained to be positive. Actually, unconstrained fits gave positive coefficients at all but a few points.

We must now specify the functions $g_i(M^2, k)$. The simplest model is that the most prominent dynamical features of the reaction are shown in the pseudo-two-

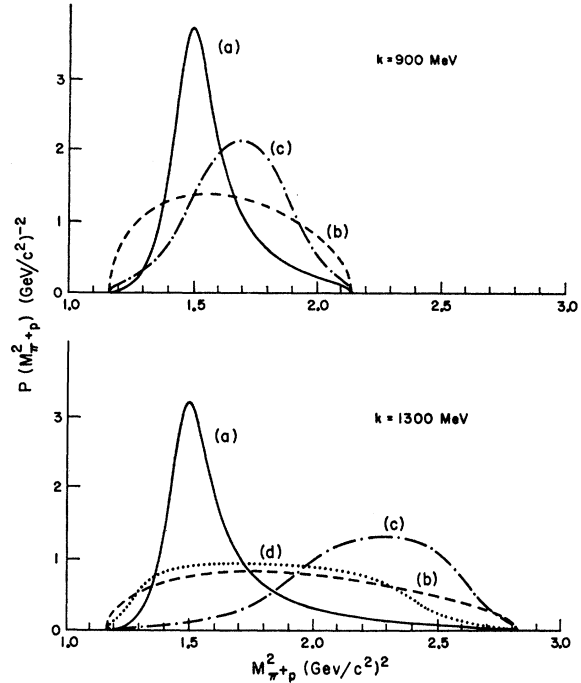


FIG. 7. Missing-mass distributions for the phenomenological model. $P(M^2)$ is the distribution function (normalized to unit area) for the square of the missing mass in $\gamma + p \rightarrow \pi^- + X$. The curves are for the specific models: (a) $\gamma + p \rightarrow \pi^- + N^*(1238)^{++}$; (b) $\gamma + p \rightarrow \pi^- + \pi^+ + p$ (nonresonant); (c) $\gamma + p \rightarrow \pi^- + N^*(1238)^0$; (d) $\gamma + p \rightarrow \rho^0 + p$. Curve (d) is not shown at 900 MeV because this is below threshold for ρ^0 production.

body channels

$$\gamma + p \rightarrow \pi^- + N^*(1238)^{++} \quad (10a)$$

$$\rightarrow \pi^- + N^*(1238)^0 \quad (10b)$$

$$\rightarrow \rho^0 + p \quad (10c)$$

and that any remaining contribution to the cross section can be described adequately by three-body invariant phase space. Rather than attempting to use dynamical models of the production mechanism to specify the M^2 dependence of reactions (10a)–(10c), we choose the phenomenological approach summarized by Jackson.¹⁴ The shape function for reaction (10a) becomes

$$g_1(M^2, k) = N \left(\frac{p'}{4W} \right) \left(\frac{M_r}{\pi} \right) \times \Gamma(M) / [(M_r^2 - M^2)^2 + M_r^2 \Gamma(M)^2], \quad (11)$$

where M_r = mass of the resonance (1238 MeV), $W(k)$ = total c.m. energy, $p'(M^2, k) = \pi^-$ c.m. momentum, N = normalization constant [although N is a slowly varying function of k , a fixed value was chosen arbitrarily and the k dependence was considered a part of $A_1(k, \theta')$], $\Gamma(M) = \Gamma_0(q/q_r)^3(\rho/\rho_r)$, Γ_0 = width parameter (123 MeV), $q = \pi^+$ 3-momentum in the (π^+p) c.m.

¹⁴ J. D. Jackson, *Nuovo Cimento* 34, 1644 (1964).

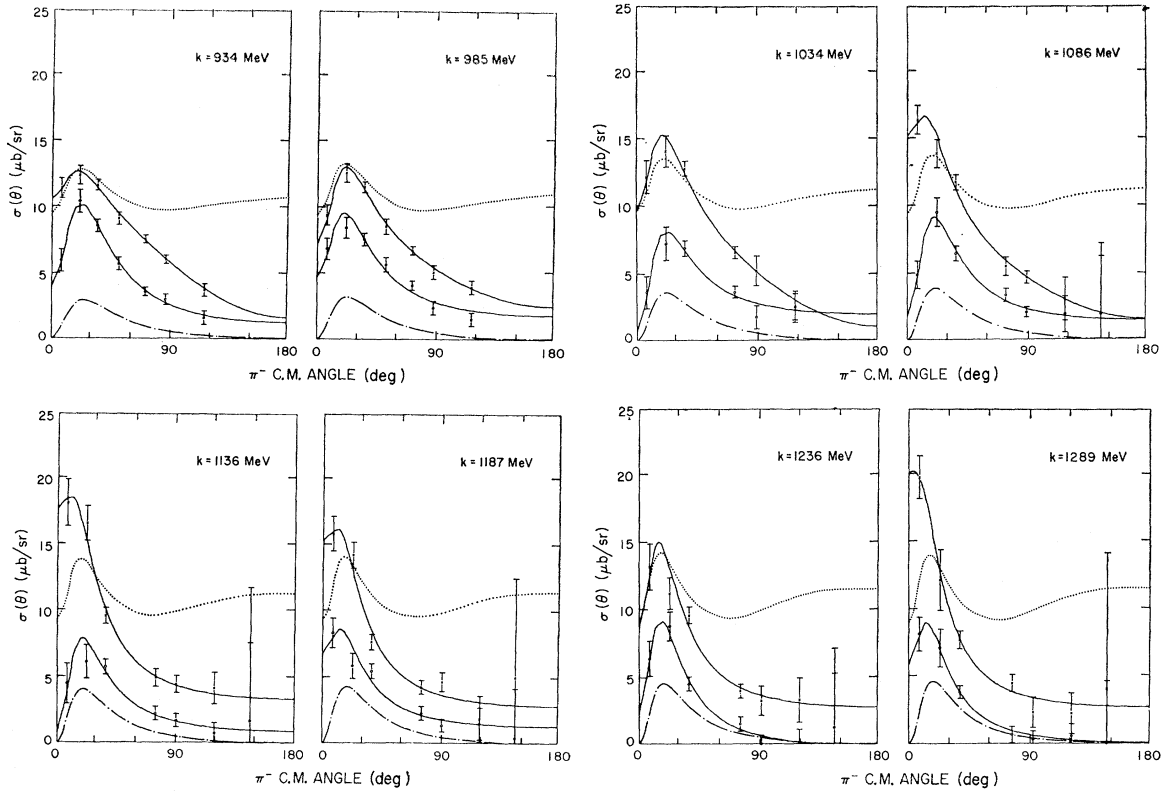


FIG. 8. Production angular distributions for negative pions in the c.m. system. The upper points at each energy (\times) are for all charged-pion-pair photoproduction, and the lower points (\circ) are for $\pi^- + N^*(1238)^{++}$ production. The solid curves are Moravcsik fits to the corresponding sets of data. The dot-dash curves are calculated from the Drell model, and the dotted curves are calculated from the Stichel-Scholz model. k is the incident photon energy in the laboratory system.

system, $\rho = [(M + M_p)^2 - m^2]/M^2$, M_p = proton mass, m = pion mass, and the subscript r denotes quantities evaluated at the resonance mass. The mass distribution from three-body invariant phase space is given simply by

$$g_2(M^2, k) = \frac{\pi p' q}{4 W M}. \quad (12)$$

Shape functions for reactions (10b) and (10c) were obtained by inserting a Breit-Wigner shape for the invariant-mass distribution of the resonant pair of particles into the integrand of the invariant-phase-space integral for the $(\pi^- \pi^+ p)$ system.

Figure 7 shows these mass distributions for two different photon energies. Because the curve representing the "reflection of the ρ^0 " is so similar to the non-resonant phase-space curve, the ρ^0 term was not included in the fitting function. This is also reasonable from a dynamical viewpoint, because bubble-chamber studies show that ρ^0 production is not a dominant part of the total cross section for k less than 1.3 GeV.^{4,5} The N^{*0} term has a much more striking mass spectrum than the ρ^0 term; however, this term also was not included in the fitting function finally used. There were

three reasons for this decision: (1) Bubble-chamber studies of the $(\pi^- p)$ mass distribution in this reaction find no significant enhancement in the $N^*(1238)^0$ region. (2) The N^{*0} term produces a peak in the $(\pi^+ p)$ mass distribution close to the maximum kinematically allowed $(\pi^+ p)$ mass, whereas our measurements were made within 250 MeV/ c^2 of the minimum possible mass. For $k \gtrsim 1$ GeV, the N^{*0} term peaks well above the maximum missing mass for which the cross section was measured, and is quite flat over the measured range. (3) The data at $k=934$ MeV, where this term seems most likely to be apparent in our measurements, were fit with an expansion including the N^{*0} term; its coefficient was consistent with zero at every angle.

Thus, the final fits were made using only two terms in Eq. (8): the N^{*++} term and three-body phase space. The upper smooth curve in each plot of Fig. 6 is the complete fitting function; the lower curve is the non-resonant part. It was found that this model fits the data well at all angles and energies. Although the peak in the resonance term occurs at 1222 MeV and its full width is 90 MeV, the observed location of the peak and the observed width generally coincide closely with the fitting function. Such differences between the observed properties of a resonant peak in a production reaction

TABLE I. Differential cross sections in the c.m. system. θ' is the π^- c.m. angle and k is the photon energy in the laboratory. $\sigma_R(k, \theta')$ is the cross section for the pseudo-two-body reaction $\gamma + p \rightarrow \pi^- + N^*(1238)^{++}$. $\sigma_C(k, \theta')$ is the cross section for all charged pion-pair photoproduction, $\gamma + p \rightarrow \pi^- + \pi^+ + p$, including both N^{*++} production and nonresonant production.

θ' (deg)	k (MeV)	$\sigma_R(k, \theta')$ ($\mu\text{b/sr}$)	$\sigma_C(k, \theta')$ ($\mu\text{b/sr}$)	θ' (deg)	k (MeV)	$\sigma_R(k, \theta')$ ($\mu\text{b/sr}$)	$\sigma_C(k, \theta')$ ($\mu\text{b/sr}$)
7.1	936	5.9±0.8	11.4±0.8	71.6	934	3.5±0.3	7.6± 0.3
7.2	985	6.8±0.8	9.4±0.8	72.6	983	4.1±0.3	6.7± 0.3
7.3	1034	3.6±1.2	12.2±1.2	73.6	1033	3.6±0.4	6.5± 0.4
7.4	1086	4.8±1.0	16.5±1.1	74.2	1085	3.3±0.5	5.4± 0.7
7.5	1136	4.5±1.5	18.3±1.8	75.0	1135	2.2±0.5	4.9± 0.7
7.7	1187	8.3±1.1	15.9±1.3	75.8	1188	2.2±0.5	4.2± 0.5
7.8	1236	6.4±1.3	13.2±1.7	76.6	1236	1.5±0.5	3.9± 0.5
7.9	1289	8.2±1.3	19.9±1.6	77.4	1285	0.7±0.6	4.5± 0.6
21.2	935	10.5±0.9	12.4±0.7	87.6	932	2.9±0.4	6.0± 0.3
21.6	983	8.5±0.8	12.7±0.7	88.7	981	2.4±0.5	5.1± 0.5
21.9	1034	7.2±1.2	14.1±1.2	89.5	1032	1.7±0.9	5.2± 1.1
22.1	1086	9.5±1.1	13.9±1.1	90.2	1082	2.0±0.4	4.6± 0.4
22.5	1135	6.1±1.3	16.7±1.3	91.0	1133	1.7±0.5	4.4± 0.6
22.8	1188	5.8±0.9	14.3±1.0	91.7	1184	1.3±0.5	4.6± 0.7
23.1	1236	8.8±1.1	11.3±1.2	92.5	1234	0.0±0.6	3.2± 1.1
23.4	1287	7.1±1.4	12.2±2.3	93.3	1283	0.3±0.6	2.3± 1.1
34.8	936	8.6±0.5	11.7±0.4	117.2	932	1.5±0.5	3.7± 0.5
35.4	984	7.6±0.5	11.6±0.4	118.1	982	1.5±0.5	3.9± 0.5
35.8	1036	6.8±0.6	12.8±0.6	118.7	1033	2.5±1.0	2.5± 1.2
36.3	1086	6.4±0.6	11.8±0.6	119.5	1082	1.8±1.3	3.0± 1.6
36.8	1139	5.7±0.6	9.6±0.6	120.0	1135	0.7±0.8	4.1± 1.2
37.3	1187	5.4±0.5	7.6±0.6	120.7	1184	1.5±1.2	1.8± 1.7
37.8	1239	4.5±0.5	9.6±0.6	121.5	1233	0.1±0.9	3.3± 1.6
38.3	1289	3.8±0.5	7.7±0.7	121.9	1287	0.6±0.9	2.2± 1.5
51.1	935	5.6±0.5	9.1±0.5	146.6	1082	1.9±4.3	1.9± 5.3
51.8	984	5.6±0.5	8.6±0.6	147.1	1131	1.6±6.0	1.6±10.2
				147.6	1180	0.4±3.7	5.0± 7.6
				147.9	1230	1.2±4.0	1.2± 5.9
				148.3	1283	0.0±4.7	4.1±10.2

and the theoretical parameters of the resonance are a common occurrence.¹⁴

The π^- c.m. differential cross section is defined as follows:

$$\sigma_i(k, \theta') = \int_{M_{\min}^2}^{M_{\max}^2} dM^2 \left(\frac{d^2\sigma'}{dM^2 d\Omega'} \right)_i, \quad (13)$$

where the integrand is the i th term from the right-hand side of Eq. (7). M_{\max} and M_{\min} are, respectively, the maximum and minimum possible values of M . Although our measurements do not extend over this entire missing-mass range, the fitting functions are well-defined everywhere and go smoothly to zero at the kinematic limits. The differential cross sections are listed in Table I, and are plotted as angular distributions at fixed energy in Fig. 8. The upper set of points in each plot is the sum of the N^{*++} and phase-space terms, the lower set, the N^{*++} term alone.

D. Total Cross Section

The total cross section for π^- production is defined in the standard manner:

$$\sigma_i(k) = \int d\Omega' \sigma_i(k, \theta'). \quad (14)$$

In order to carry out the integral, smooth curves were

fitted to the angular distributions. Since the OPE diagram was expected to make an important contribution to the cross section, we followed Moravcsik's suggestion and performed a fit in the following manner¹⁵:

$$(1 - \beta_r x)^2 \sigma(k, \theta') = \sum_{j=0}^n B_j x^j, \quad (15)$$

where $x = \cos\theta'$, $\beta_r = \pi^-$ c.m. velocity for which the missing mass is equal to 1238 MeV/ c^2 . Fake data points were included at c.m. angles of 150° and 180° in order to constrain the Moravcsik fits to be well behaved at backward angles. The values of the cross section at these points were taken equal to the measured value at 120°, and the error bars included zero. This trick seems justified since the bubble-chamber studies show the angular distributions to be quite flat for backward π^- angles from 0.85 to 1.5 GeV.⁴

The smooth curves in Fig. 8 are the Moravcsik fits used to obtain the total cross sections. Both the complete total cross section and its resonant part are generally independent of the order of the fit for $n \geq 3$. The Moravcsik coefficients and the total cross sections are listed in Table II, and the cross sections are plotted in Fig. 9.

¹⁵ M. J. Moravcsik, Phys. Rev. **104**, 1451 (1956).

TABLE II. Results of the Moravcsik fits to the c.m. angular distributions. k is the photon energy in the laboratory. The B_i are the coefficients obtained in the Moravcsik fits to the differential cross sections for the reactions indicated [see Eq. (15)]. $\sigma_R(k)$ and $\sigma_C(k)$ are the total cross sections for the respective reactions. λ is the πN^* coupling constant obtained by extrapolation of the Moravcsik fit to the N^* production data. The errors for the B_i are the statistical errors obtained in the least-squares fitting procedure; the errors in the total cross sections and λ are those implied by the errors in the B_i , taking into account the correlations between the B_i determined in each fit.

k (MeV)	934	985	1034	1086	1136	1187	1236	1289
$\gamma + p \rightarrow \pi^- + N^*(1238)^{++}$								
B_0 ($\mu\text{b}/\text{sr}$)	2.58 ± 0.23	2.80 ± 0.24	2.74 ± 0.36	2.29 ± 0.29	1.59 ± 0.26	1.77 ± 0.32	0.66 ± 0.32	0.65 ± 0.33
B_1 ($\mu\text{b}/\text{sr}$)	-2.25 ± 0.55	-3.32 ± 0.56	-3.56 ± 0.82	-2.65 ± 0.67	-1.63 ± 0.59	-2.35 ± 0.71	0.20 ± 0.71	-0.14 ± 0.74
B_2 ($\mu\text{b}/\text{sr}$)	-0.30 ± 0.34	0.55 ± 0.34	0.82 ± 0.48	0.37 ± 0.40	0.04 ± 0.35	0.60 ± 0.41	-0.86 ± 0.41	-0.50 ± 0.43
σ_R (μb)	45.0 ± 2.4	45.9 ± 2.5	42.9 ± 3.8	39.1 ± 3.2	29.2 ± 3.0	30.8 ± 3.5	19.9 ± 3.5	18.2 ± 3.5
$\lambda^2/4\pi$ (GeV^{-2})	32.0 ± 3.2	24.2 ± 3.1	24.8 ± 4.2	25.9 ± 3.8	23.0 ± 4.2	13.2 ± 3.9	25.0 ± 4.2	16.9 ± 4.5
$\gamma + p \rightarrow \pi^- + \pi^+ + p$								
B_0 ($\mu\text{b}/\text{sr}$)	5.83 ± 0.21	5.36 ± 0.25	5.09 ± 0.42	4.67 ± 0.36	4.33 ± 0.42	3.65 ± 0.39	3.69 ± 0.45	3.49 ± 0.50
B_1 ($\mu\text{b}/\text{sr}$)	-5.94 ± 0.80	-6.24 ± 0.89	-4.56 ± 1.57	-4.81 ± 1.47	-6.23 ± 0.96	-5.30 ± 0.88	-5.26 ± 1.02	-5.24 ± 1.15
B_2 ($\mu\text{b}/\text{sr}$)	-2.87 ± 1.40	-0.70 ± 1.50	-3.17 ± 2.54	-1.86 ± 2.69	1.95 ± 0.55	1.69 ± 0.50	1.59 ± 0.58	1.78 ± 0.67
B_3 ($\mu\text{b}/\text{sr}$)	3.06 ± 0.76	1.62 ± 0.80	2.69 ± 1.31	2.06 ± 1.44				
σ_C (μb)	78.9 ± 2.9	76.9 ± 3.3	75.3 ± 5.7	71.5 ± 5.0	71.4 ± 4.5	60.6 ± 4.2	61.1 ± 4.8	59.1 ± 5.2

These total cross sections are to some extent model-dependent, since the quantities $\sigma_i(k, \theta')$ are model-dependent. Only the shape of our phenomenological model determined the cross section for missing-mass values where no measurements were made. The fraction of the complete pion-pair total cross section which comes from the missing-mass range covered by the measurements varies smoothly from about $\frac{3}{4}$ at the lowest energy to $\frac{1}{2}$ at the highest energy. The fractions for the N^{*++} term alone are $\frac{7}{8}$ and $\frac{3}{4}$ at the same energies.

E. Errors

In this section we summarize the factors affecting the precision and accuracy of the measurements. The dominant source of random error in our results was counting statistics: Although the yield per equivalent quantum was generally measured with 5%–10% statistical error per spectrometer channel, the bremsstrahlung subtraction amplified this by a sizeable factor. Other sources of random error, such as beam monitoring and the energy stability of the synchrotron, contributed a 1.4% rms fluctuation in the yield, which was included in quadrature with the counting error in all results.

The estimated accuracy of our absolute normalization is 7%. The major sources of systematic error common to the data from both spectrometers include the nuclear absorption correction (3–4%), the absolute quantameter calibration (3%), counter and electronic efficiency (2%), the shape of the bremsstrahlung spectrum (2%), and contamination from three-pion production (2%). In addition, there was an estimated 2–5% electron contamination of the 600-MeV/c-spectrometer data. The normalization of the yields measured with the 1200-MeV/c spectrometer differed by 4% in the two running periods of this experiment. This difference apparently resulted from a small change made in the horizontal dimension of the aperture-defining counter of the spectrometer, but we were

unable to explain the effect quantitatively. Since yields measured simultaneously with both spectrometers at the same kinematic point during the second running period were in good agreement, the earlier cross sections measured with the 1200-MeV/c spectrometer were renormalized by 4% before the results from the two running periods were averaged. An error of 4% has been included in our estimate of the normalization accuracy in recognition of the uncertainty in this procedure.

V. DISCUSSION

A. Comparison with Other Experiments

The data presented in the previous sections show clearly the important role played by the pseudo-two-body channel $\gamma + p \rightarrow \pi^- + N^*(1238)^{++}$ in photoproduction of charged pion pairs from 0.9 to 1.3 GeV. This is perhaps most evident in the π^- momentum spectra of Fig. 6. The difference between the smooth curves shown in this figure is the contribution of the $N^*(1238)^{++}$.

In order to compare our results with previous work, the total cross sections obtained in other recent experiments have been plotted in Fig. 9. Both the complete cross section for pion-pair production and the total cross section for $N^*(1238)^{++}$ production determined in this experiment are in good agreement with the CEA and DESY bubble-chamber data. This agreement suggests that the model we used to extrapolate our measurements over the unobserved missing-mass range did not introduce serious errors.

There seems to be substantial agreement between our results and the Stanford results for the resonant part of the total cross section, but there is significant disagreement on the complete total cross section. Although their experimental method was essentially identical to ours, they analyzed their data in a different manner. Their approach, in which they fit the yield at fixed momentum as a function of the bremsstrahlung end-

point energy, required that they make an arbitrary choice of normalization for the nonresonant part of the cross section. Since the nonresonant fraction of the cross section increases as k increases, one would expect a normalization error to affect their cross section most at the highest k they observed, which is just where our experiments overlap. Since the DESY and CEA results are closer to ours in this region, we are inclined to believe that the Stanford group underestimated the nonresonant part of the cross section. This interpretation is consistent with the fact that our experiments get the same result for the N^* total cross section, since there was no arbitrariness in their normalization of the N^* term.

B. Contribution of the $N^*(1688)$

The total cross sections show a smooth decrease as k increases, with no appreciable structure near 1.05 GeV where the $N^*(1688)$ shows up in single-pion photoproduction. There may be a slight shoulder in the cross section in this region, particularly in the N^* cross section, but to say this with any confidence we must believe that the normalizations of the Stanford data and our data are consistent. It is interesting to estimate the magnitude we might expect for the $N^*(1688)$ contribution to $N^*(1238)^{++}$ production. Ecklund and Walker¹² found that the $N^*(1688)$ has a peak total cross section of 25 μb in the reaction $\gamma + p \rightarrow \pi^+ + n$. Lovelace¹⁶ gives partial widths for this state (predominantly $F_{5/2}$ in photoproduction) of 69 MeV for elastic channels and 35 MeV for inelastic channels, with $\pi N^*(1238)$ being the dominant inelastic channel. If we assume all the inelastic decays are in the $\pi N^*(1238)$ channel, isotopic spin arguments predict a total cross section of about 10 μb in $\pi N^*(1238)^{++}$ photoproduction. The data seem consistent with a contribution of this magnitude.

We could also search for evidence of $N^*(1688)$ formation in the production angular distributions. However, the limited number of data points available in each angular distribution prevent us from introducing as many parameters into our analysis as the description of such a process demands. Our data show that the one-pion-exchange mechanism plays a dominant role in $N^*(1238)$ production in our energy range; more detailed measurements are needed to determine the nature and magnitude of additional contributions.

C. Comparison with the OPE Model

We turn now to comparison of our results with predictions of the one-pion-exchange model. If we use the pole approximation to evaluate the amplitude for the diagram in Fig. 1, we obtain the following invariant

¹⁶ C. Lovelace, in *Proceedings of the Thirteenth International Conference on High-Energy Physics, Berkeley, 1966* (University of California Press, Berkeley, California, 1967).

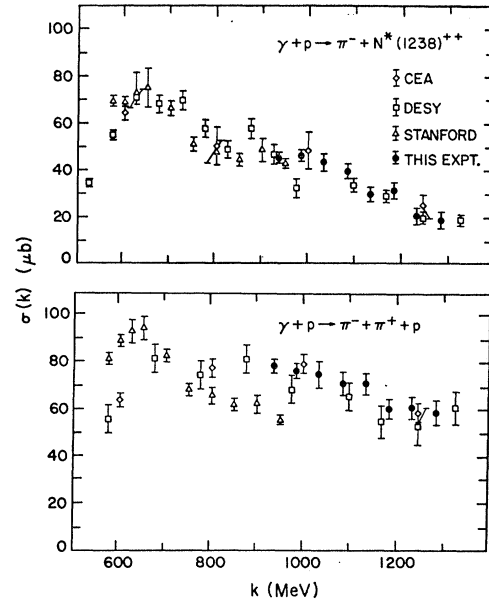


FIG. 9. Total cross sections for $\gamma + p \rightarrow \pi^- + N^*(1238)^{++}$ and $\gamma + p \rightarrow \pi^- + \pi^+ + p$. k is the incident photon energy in the laboratory system. The data from CEA, DESY, and Stanford are from Refs. 4-7.

cross section:

$$\frac{d^2\sigma}{dM^2 dt} = \frac{2\alpha}{\pi} \frac{qM}{(W^2 - M_p^2)^2} \frac{1}{(t - m^2)^2} \times \frac{1}{2} \sum_{\mu} |\epsilon^{\mu} \cdot p|^2 \sigma_{\pi p}(M), \quad (16)$$

where α = fine-structure constant, $t = (p - k)^2$, ϵ^{μ} = polarization 4-vector of the photon, p = 4-momentum of the external pion at the electromagnetic vertex, k = 4-momentum of the photon, $\sigma_{\pi p}(M)$ = total (πp) scattering cross section at a (πp) c.m. energy of M . If we choose the Coulomb gauge in the c.m. system, the sum over photon polarizations is just $(p' \sin\theta')^2$, and Eq. (16) is equivalent to the Drell cross section except for kinematic factors of order unity which Drell ignored for the purposes of his argument.² Although this expression ignores various kinematic and dynamic off-shell correction factors which have been suggested,¹⁷ we shall compare its predictions with the data.

We are interested in Eq. (16) for M values near threshold, where $\sigma_{\pi p}(M)$ is dominated by scattering in the $I = \frac{3}{2}, J = \frac{3}{2}$ state. Since $\sigma(\pi^+ p \rightarrow \pi^+ p) / \sigma(\pi^- p \rightarrow \pi^- p) = 9$ for scattering in a pure $I = \frac{3}{2}$ state, this model predicts a 9:1 ratio for $N^*(1238)^{++}$ production relative to production of the $N^*(1238)^0$ followed by decay into the $(\pi^- p)$ charge state. This is consistent with the absence of an N^{*0} enhancement, both in our data and the bubble-chamber data. This prediction is not unique to the OPE model: The same conclusion is reached if

¹⁷ M. L. Thiebaut, *Phys. Rev. Letters* **13**, 29 (1964).

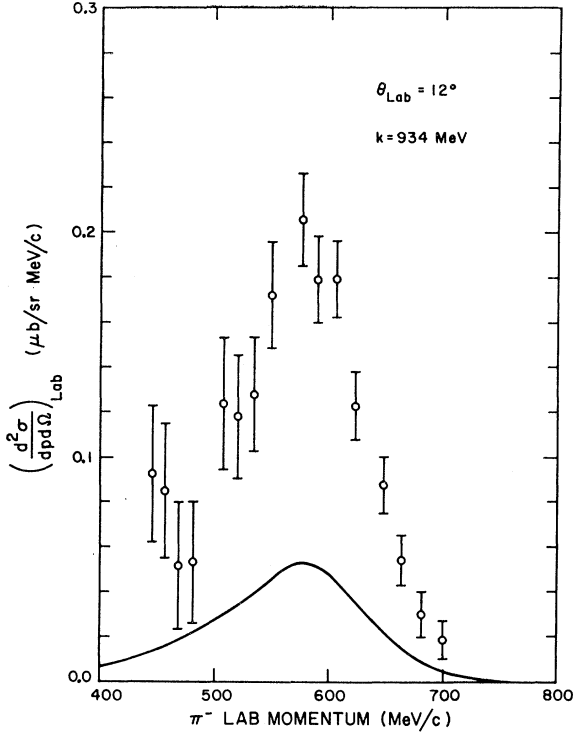


Fig. 10. Comparison of a measured π^- momentum spectrum with the spectrum calculated from the Drell model. The bremsstrahlung spectrum has been folded into the calculated curve.

one supposes the reaction to occur in a pure $I=\frac{1}{2}$ state. From this point on, we shall consider only the OPE diagram where the π^- is produced at the electromagnetic vertex.

The π^- momentum spectrum given by Eq. (16) is compared with one of our experimental spectra at a point where the N^{*++} is dominant in Fig. 10. The bremsstrahlung spectrum has been folded into the theoretical cross section. As Kilner, Diebold, and Walker³ observed, the qualitative shape of the Drell cross section resembles the data very closely.

One of the most characteristic features of the OPE model is the angular distribution of the π^- . The c.m. angular distributions calculated by integrating Eq. (16) over all kinematically allowed M^2 are shown with the data in Fig. 8. The shape of the Drell curve is strikingly similar to the behavior of the data, particularly the N^* part. The N^* data show the decrease in cross section predicted for $\theta < m/p_r'$ (p_r' is the π^- c.m. momentum for $M=1238$ MeV/ c^2), as well as the rapid decrease at larger angles.

Since the data show a strong influence of the pole term, it is interesting to extrapolate the Moravcsik fits to the pion pole. The residue at the pole can be related to the πNN^* coupling constant λ . We have done this by calculating the differential cross section for production of a stable $N^*(1238)^{++}$ from the diagram in Fig. 11(a), assuming a πNN^* coupling of the form λq_α ,

where q is the four-momentum of the exchanged pion. The result in the c.m. system can be expressed in the form

$$\frac{d\sigma}{d\Omega'}(\theta') = \left(\frac{\lambda^2}{4\pi}\right) \left(\frac{2\alpha}{3}\right) \times \frac{\sin^2\theta'}{(t-m^2)^2} \frac{p'^3 M_p^3 M}{k' W^2} (\Lambda+1)^2 (\Lambda-1), \quad (17)$$

where k' = photon c.m. energy, p', θ' = π^- c.m. 3-momentum and angle, respectively, $\Lambda = (M_p^2 + M^2 - t)/2MM_p$, and all quantities are evaluated at $M=M_r=1238$ MeV/ c^2 . The coupling constants ($\lambda^2/4\pi$) obtained from the Moravcsik fits to the N^* data are listed in Table II. The extrapolation makes the coupling constant quite sensitive to the form of the fitting function. We found that changing the number of terms used in the Moravcsik expansion by one from the value used in Table II typically changes the coupling constant by an amount comparable to its statistical error. It is therefore not surprising that the coupling constants obtained at different energies show greater fluctuations than expected solely from their statistical errors. Choosing the standard deviation of the mean of the observed values as the experimental uncertainty, our average coupling constant $\lambda^2/4\pi = (23.1 \pm 2.0)$ GeV $^{-2}$ is in fair agreement with the value obtained from the width of the N^* :

$$\frac{\lambda^2}{4\pi} = \frac{3M_r\Gamma_r}{q^3(E+M_p)} \cong 19.1 \text{ GeV}^{-2}, \quad (18)$$

where $q = \pi^+$ three-momentum in the N^* rest frame, $E = p$ total energy in the N^* rest frame, $\Gamma_r = 123$ MeV.

In addition to these impressive successes, the OPE model has some deficiencies. It does not give the correct energy dependence for the total cross section; this is

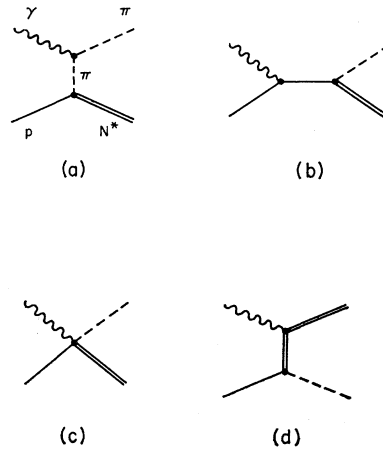


Fig. 11. Diagrams used in the gauge-invariant Born approximation.

apparent to some extent in our data, and is even more evident in the wider energy range covered by the bubble-chamber data. Both DESY and CEA bubble-chamber collaborations have found that the model does not correctly describe the distribution of the N^* decay angles.

From a theoretical point of view, the OPE model alone is not acceptable because it is not gauge-invariant. A gauge-invariant Born approximation has been calculated using the four diagrams shown in Fig. 11,¹⁸ treating the N^* as a stable particle. Even when the coupling of the photon to the anomalous moments of the nucleon and the N^* is neglected, the calculated cross section is in serious disagreement with the observed π^- angular distributions in N^* production, being generally too large and increasing to very large values in the backward direction. Stichel and Scholz also performed a gauge-invariant calculation, but included only parts of the amplitudes from diagrams 11(b) and 11(d).¹⁹ Angular distributions calculated from the Stichel-Scholz amplitude using $\lambda^2/4\pi = 19.1 \text{ GeV}^{-2}$ are shown in Fig. 8. These curves do not drop off as rapidly

as the data on either side of the peak at small angles, and are generally too large in magnitude.

We conclude that the OPE model predicts many of the qualitative features of pion-pair photoproduction quite well, particularly in the pseudo-two-body channel $\gamma + p \rightarrow \pi^- + N^*(1238)^{++}$. However, a considerable amount of analysis remains to be done if we are to have a quantitative understanding of pion-pair production within the framework of a gauge-invariant theory.

ACKNOWLEDGMENTS

I wish to acknowledge the contribution of my advisor, Professor R. L. Walker, who originally proposed this investigation and provided many helpful suggestions. This experiment received a large amount of technological fallout from the work of Dr. H. A. Thiessen and Dr. S. D. Ecklund. I also wish to thank Dr. Thiessen for assistance in the collection of data. The assistance of the technical crew of the synchrotron was greatly appreciated. I am grateful to Professor J. Mathews for many helpful discussions and calculations relating to interpretation of the data. Finally, I wish to acknowledge the financial support of the National Science Foundation and the Atomic Energy Commission.

¹⁸ J. Mathews (private communication).

¹⁹ P. Stichel and M. Scholz, *Nuovo Cimento* **34**, 1381 (1964).

Multiple Particle Production in 22.8-GeV/c Proton-Nucleon Interactions*

B. BHOWMIK AND R. K. SHIVPURI

Department of Physics and Astrophysics, University of Delhi, Delhi, India

(Received 28 November 1966; revised manuscript received 8 May 1967)

The aim of the present work is to study the contribution of baryon excited states to multiple particle production. The interactions have been divided into two categories, viz., those having shower multiplicity less than or equal to four and those having multiplicity greater than four. The features that have been studied are the angular distribution, inelasticity, transverse momentum, and center-of-mass momentum of protons and pions. It has been found that the characteristics of high-multiplicity events are well accounted for on the basis of the statistical theory, whereas those of low-multiplicity events can be well explained by considering the final-state particles as decay products of isobars. The results indicate the probable dominance of isobars having isospin $\frac{1}{2}$.

I. INTRODUCTION

THE study of high-energy proton-nucleon interactions has been carried out by a large number of investigators at primary momenta of 1–25 GeV/c. The first theoretical attempt to explain the observed features of particle production was advanced by Fermi,¹ who suggested that statistical ideas could be applied to describe the multiple-particle production processes at

high energies. The theory was modified by Kovacs² to include the final-state interactions between the particles, and in particular the pion-nucleon interaction in the $T=J=\frac{3}{2}$ state and the nucleon-nucleon interaction. Although the modified form improved the predictions of the statistical theory, it could not explain satisfactorily all the observed features of the particle production. The observation of a strong pion-nucleon interaction in π - p scattering led Lindenbaum and Sternheimer³ to conclude that the pion proceeds via the

* A preliminary report of this work was presented at the Oxford International Conference on Elementary Particles, 1965 (unpublished).

¹ E. Fermi, *Progr. Theoret. Phys. (Kyoto)* **5**, 570 (1950); *Phys. Rev.* **92**, 452 (1953); **93**, 1435 (1954).

² J. S. Kovacs, *Phys. Rev.* **101**, 397 (1956).

³ S. J. Lindenbaum and R. M. Sternheimer, *Phys. Rev.* **105**, 1874 (1957); **123**, 333 (1961).